# Supporting Information

## Enhanced thermoelectric figure of merit and heat-electricity efficiency in *p*-type $Mm_{0.8}Fe_{2.7}Co_{1.3}Sb_{12}$ skutterudites *via* polyaniline compositing

Xiaofang Cao[‡a], Fudong Zhang[‡a], Mingzhen Song[a], Xiaohui Pang[a], Xiaolian Chao[a], Zupei Yang[*a], Di Wu[*a]

[a] *Key Laboratory for Macromolecular Science of Shaanxi Province and Shaanxi Key Laboratory for Advanced Energy Devices, School of Materials and Engineering, Shaanxi Normal University, Xi'an, 710062, PR China*

[*] Corresponding author

*E-mail addresses*: yangzp@snnu.edu.cn (Z. Yang), wud@snnu.edu.cn (D. Wu)

[‡] These authors contributed equally to this work.

# 1. Materials and methods

## 1.1 Sample synthesis

Firstly, we synthesized a series of $Mm_{0.8}Fe_{2.7}Co_{1.3}Sb_{12}$ samples. Mm (Misch metal, Ce 50wt%, La 25wt%, Nd 20wt%, Pr 5wt%, 99.0%, Aex), Fe (99.99%, Aex), Co (99.99%, China New Metal), and Sb (99.999%, Aladdin) particles were weighed in carbon-plated quartz tubes according to the stoichiometric ratios, then vacuum sealed and slowly heated to 1100°C in a muffle furnace, held for twelve hours, quenched in cold water, and then annealed at 650°C for seven days. The obtained ingots were first ground into small pieces in an agate mortar and then the $Mm_{0.8}Fe_{2.7}Co_{1.3}Sb_{12}$/(*x wt*% PANI) mixtures with different mass ratios (*x* = 0, 0.25, 0.50, 0.75, 1.00 *wt*%) were weighed, ground into powder in the mortar, loaded into a graphite model with a diameter of 15 mm, and sintered for 13 min at a temperature of 650°C and an axial pressure of 50 MPa using a spark plasma sintering system (LABOX-212, Japan). The resulting blocks were then cut into 2 × 2 × 12 $mm^3$ rectangles for electrical property tests and into 6 × 6 × 2 $mm^3$ plates for thermal diffusivity tests.

## 1.2 Structural characterization and thermoelectric performance testing

The phase composition of all samples was determined by X-ray diffractometer (XRD, MiniFlex 600, Ragaku, Japan) with an excitation voltage of ~ 40 kV and a current of ~ 15 mA. The surface morphology of the samples was tested by scanning electron microscope (SEM, SUB8020, Japan) and the corresponding elemental distribution was analyzed by the equipped energy dispersive spectrometer (EDS). The spectral range of the Fourier transform infrared spectrometer (FTIR) is 4000 - 400 $cm^{-1}$(PerKinElmer UATR). Raman spectroscopy was conducted using the confocal micro-Raman system (Renishaw inVia Reflex).

The Seebeck coefficient and conductivity were measured with a commercial instrument (ADVANCE RIKO ZEM-3, Japan) under dilute argon atmosphere, and the experimental error for each parameter was expected to be within 5%. The total thermal conductivity was calculated from the equation

$$\kappa_{tot} = D\rho C_P \qquad \text{* MERGEFORMAT (1.1)}$$

where $D$, $\rho$, $C_p$ are the thermal diffusion coefficient, density and specific heat capacity, respectively. The thermal diffusion coefficient was obtained using the laser pulse method (NETZSCH, LFA467, Germany) tested under nitrogen atmosphere protection with an uncertainty within 5%; the mass densities was measured using the Archimedes method, and the specific heat capacity was derived from the Dulong-Petit law. The electronic thermal conductivity was calculated using the Wiedemann-Franz law

$$\kappa_e = L\sigma T \qquad \text{* MERGEFORMAT (1.2)}$$

where L is the Lorentz constant, using the formula[1]

$$L = 1.5 + exp(-|S|/116) \qquad \text{* MERGEFORMAT (1.3)}$$

Formula for using lattice thermal conductivity is

$$\kappa_{lat} = \kappa_{tot} - \kappa_e \qquad \text{* MERGEFORMAT (1.4)}$$

The total uncertainty of all the measurements involved in the calculation of $ZT$ was less than 12%. The room temperature carrier concentration and carrier mobility were measured using the van der Pauw method (Lake Shore 8400 Series, USA).

**1.3 Finite Element Simulation**

The theoretical maximum output efficiency of our synthesized material were evaluated by utilizing multi-physics finite element simulation in COMSOL program. We constructed a thermoelectric three-dimensional module, including *n*- and *p*-type legs, Cu electrodes and ceramic substrates. The *n*-type $Al_{0.03}Yb_{0.25}Co_4Sb_{12}$[2] and *p*-type $Mm_{0.8}Fe_{2.7}Co_{1.3}Sb_{12}$ + 0.75 *wt*% PANI counterparts were used in the simulations for temperature-dependent $S$, $\sigma$, and $\kappa$. Optimization of the geometries was performed, including fixing the ratio of the cross-sectional area of the *p*-legs to the *n*-legs (Ap/An), and the ratio of the height to the total cross-sectional area (H/Apn), where Apn = Ap + An. Based on the optimized geometry, the theoretical temperature difference ΔT at different hot-side temperatures and the output efficiency at a given hot-side temperature were simulated.

## 2. Supplemental Figures and Table

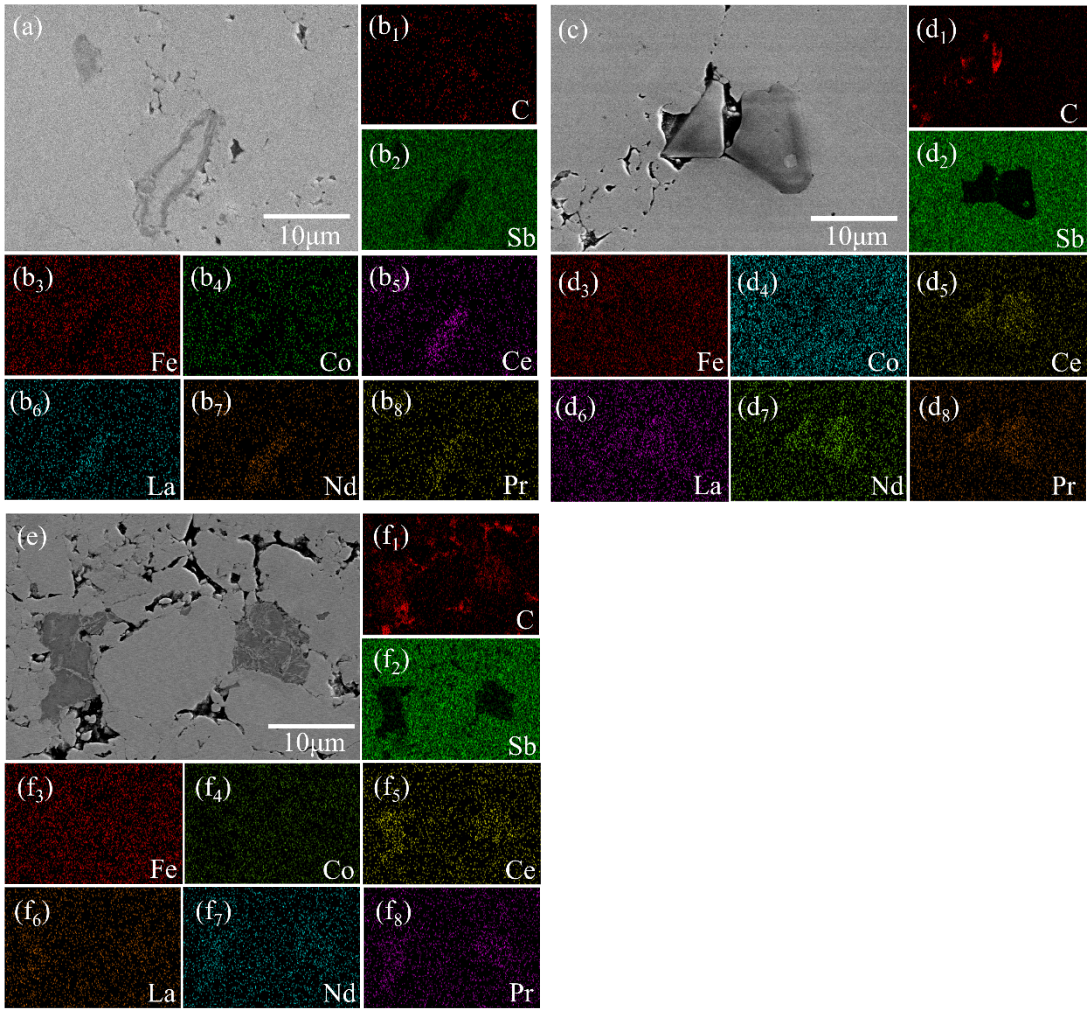


**Fig.S1** (a) SEM analysis and corresponding (b) EDS energy spectroscopy for $Mm_{0.8}Fe_{2.7}Co_{1.3}Sb_{12}$ + 0.25 *wt*% PANI sample; (c) SEM analysis and corresponding (d) EDS energy spectroscopy for $Mm_{0.8}Fe_{2.7}Co_{1.3}Sb_{12}$ + 0.50 *wt*% PANI sample; (e) SEM analysis and corresponding (f) EDS energy spectroscopy for $Mm_{0.8}Fe_{2.7}Co_{1.3}Sb_{12}$ + 1.00 *wt*% PANI sample.

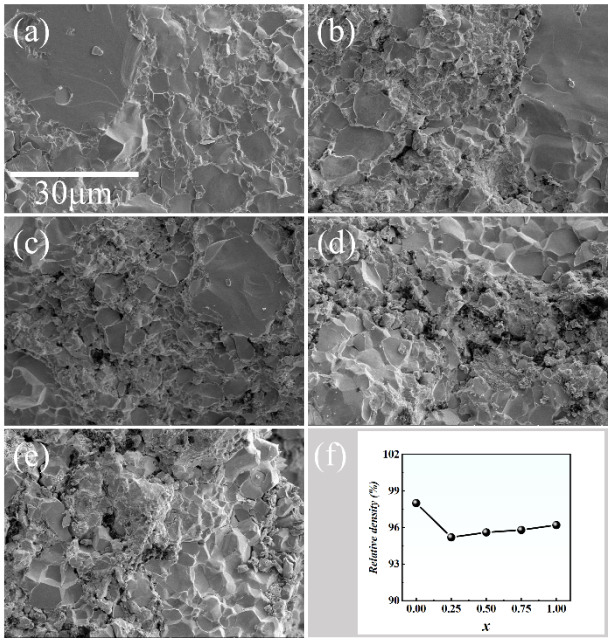


**Fig.S2** (a-e) Cross-section scans and (f) relative densities of $Mm_{0.8}Fe_{2.7}Co_{1.3}Sb_{12}$ + *x wt*% PANI (*x* = 0, 0.25, 0.50, 0.75, 1.00) samples.

Fig. S2(a-e) shows cross-sectional scans of the samples $Mm_{0.8}Fe_{2.7}Co_{1.3}Sb_{12}$ + *x wt*% PANI (where *x* = 0, 0.25, 0.50, 0.75, 1.00), revealing a progressive augmentation in amorphous morphology. Furthermore, Fig. S2(f) illustrates the relative densities of both the pristine matrix and composite samples, demonstrating a significant reduction in the relative densities of the composite samples with increasing PANI content.

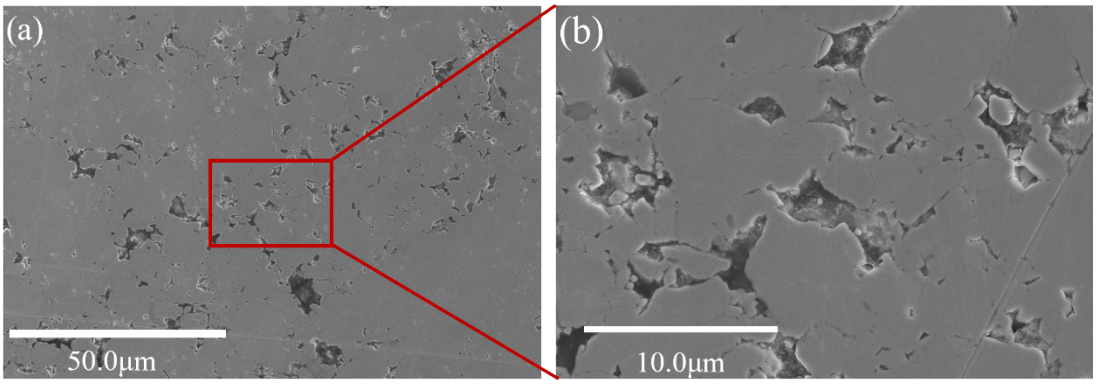


**Fig. S3** (a) SEM image of $Mm_{0.8}Fe_{2.7}Co_{1.3}Sb_{12}$ + 0.75 *wt*% PANI sample, (b) enlarged view of the red box in (a)

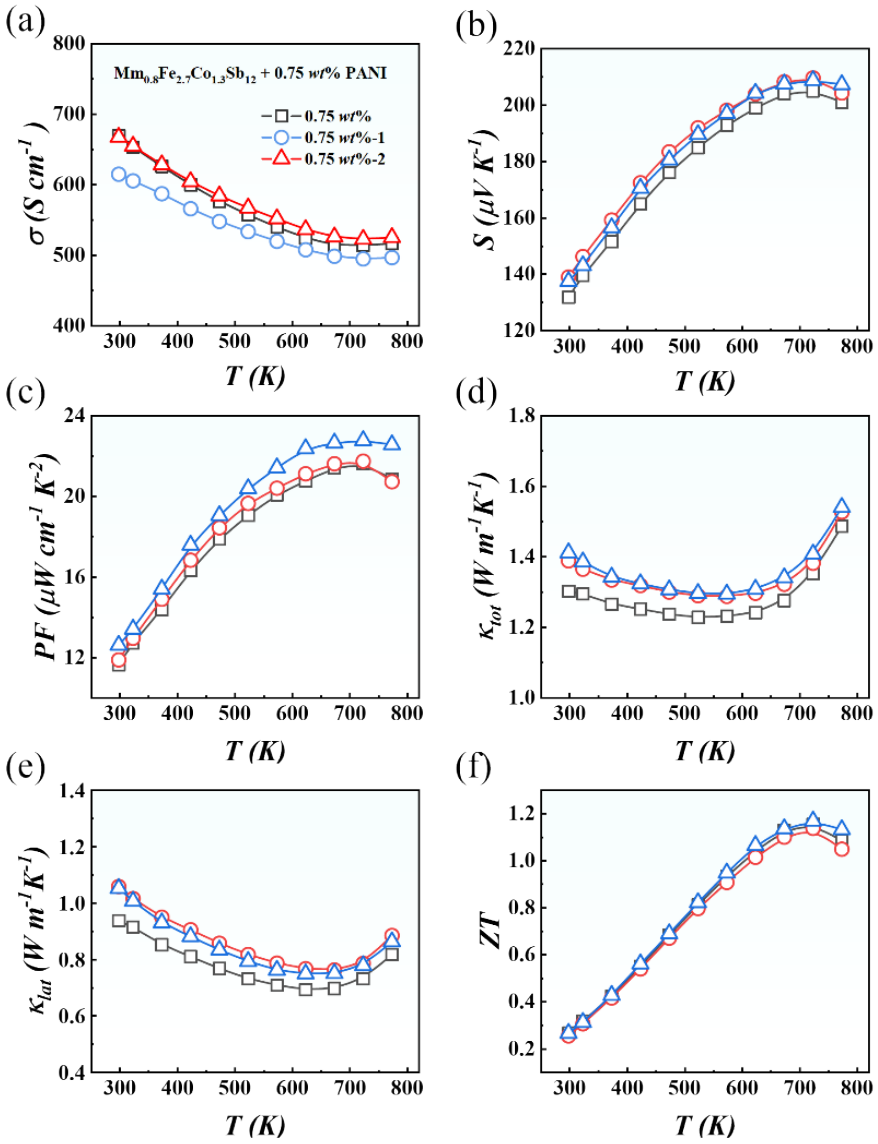


**Fig.S4** Temperature-dependent (a) electrical conductivity, (b) Seebeck coefficient, (c) power factor, (d) total thermal conductivity, (e) lattice thermal conductivity, and (f) *ZT* values for $Mm_{0.8}Fe_{2.7}Co_{1.3}Sb_{12}$ + 0.75 *wt*% PANI.

**Table S1** Conductivity, Seebeck coefficient, carrier concentration and mobility at room temperature of $Mm_{0.8}Fe_{2.7}Co_{1.3}Sb_{12}$ + *x wt*% PANI (*x* = 0, 0.25, 0.50, 0.75, 1.00) samples

| Composition | $\sigma$ ($S\ cm^{-1}$) | $S$ ($\mu V\ K^{-1}$) | $n$ ($cm^{-3}$) | $\mu_H$ ($cm^2\ V^{-1}s^{-1}$) |
|---|---|---|---|---|
| *x* = 0 | 823.63 | 133.47 | 1.19E+21 | 4.33 |
| *x* = 0.25% | 761.85 | 128.15 | 5.32E+20 | 8.96 |
| *x* = 0.50% | 687.28 | 134.65 | 6.83E+20 | 6.29 |
| *x* = 0.75% | 669.54 | 131.90 | 6.14E+20 | 6.81 |
| *x* = 1.00% | 665.85 | 133.66 | 1.10E+21 | 3.79 |

**Table S2** Rate of change in electrical and lattice thermal conductivities of the $Mm_{0.8}Fe_{2.7}Co_{1.3}Sb_{12}$ + *x wt*% PANI (*x* = 0, 0.25, 0.50, 0.75, 1.00) samples

| Composition | $\sigma$ at 773K ($S\ cm^{-1}$) | Rate of change (%) | $\kappa_{lat}$ at 623K ($W\ m^{-1}K^{-1}$) | Rate of change (%) |
|---|---|---|---|---|
| *x* = 0 | 823.63 | 0 | 1.18 | 0 |
| *x* = 0.25% | 761.85 | -3.5 | 0.96 | -18.5 |
| *x* = 0.50% | 687.28 | -11.6 | 0.90 | -23.8 |
| *x* = 0.75% | 669.54 | -15.0 | 0.69 | -41.1 |
| *x* = 1.00% | 665.85 | -14.3 | 0.78 | -33.6 |

## References


[1] H.-S. Kim, Z. M. Gibbs, Y. Tang, et al. APL Materials. 2015, 3(4): 3041506.
[2] X. Pang, M. He, F. Zhang, et al. Chemical Engineering Journal. 2024, 481: 148457.